Self-consistent Green's-function method for surfaces of random alloys

J. Kudrnovský
Institute of Physics, Czech Academy of Sciences, CS-180 40 Praha 8, Czech Republic and Institute for Technical Electrochemistry, Technical University, A-1060 Vienna, Austria

I. Turek
Institute of Physical Metallurgy, Czech Academy of Sciences, CS-616 62 Brno, Czech Republic

V. Drchal
Institute of Physics, Czech Academy of Sciences, CS-180 40 Praha 8, Czech Republic

P. Weinberger
Institute for Technical Electrochemistry, Technical University, A-1060 Vienna, Austria

S. K. Bose
Department of Physics, Brock University, Saint Catharines, Ontario, Canada L2S 3A1

A. Pasturel
Laboratoire de Thermodynamique et Physico-Chimie Métallurgiques, Ecole Nationalé Supérieure, 38402 Saint Martin d'Hères, France
(Received 23 December 1992)

An efficient self-consistent Green's-function technique using a generalization of the coherent-potential approximation method is presented in order to describe the electronic structure of inhomogeneous semi-infinite alloys with varying concentration profiles at the surface within the local-density approximation. The formalism is applied to the study of the electronic properties of the (001) surface of $Cu_{1-x}Ni_x$ fcc random alloys.

I. INTRODUCTION

Surfaces of bulk alloys are of great interest from both the theoretical and technological points of view, since many of them segregate in the near-surface region. Segregation plays an important role in catalysis, chemisorption, crystal growth, etc. An understanding of these surface phenomena requires a precise knowledge of the surface composition. Much experimental evidence has been provided by Auger-electron spectroscopy and ion-scattering spectroscopy. Theoretically, up to now, mostly phenomenological theories have been used.[1–3] An efficient way to solve the problem of segregation is the use of the Monte Carlo method[4] for a surface Ising model.[5] Recently, a first-principles formulation for the parameters in the Ising model for surface-related problems was presented[6] and successfully used to study the CuPd surface-alloy formation on the (001) surface of Cu,[7] but also for a Monte Carlo study of the surface segregation in $Cu_{1-x}Ni_x(001)$ alloys.[8]

A realistic description of the underlying electronic structure of such systems requires (i) the use of semi-infinite geometry, (ii) a self-consistent determination of the potentials and the charge densities of the alloy components in the various layers within the density-functional formalism, (iii) a proper self-consistent description of the vacuum-solid interface or the dipole barrier in order to obtain reasonable estimates for the positions of surface states, work functions, etc., and (iv) a generalization of the coherent-potential approximation (CPA) in order to treat strongly inhomogeneous systems. Only by means of a realistic description of the electronic structure of alloys with varying concentration profiles near the surface can the problem of segregation be addressed in an adequate manner. In the present paper the self-consistent Green's-function method, based on the local-density approximation (LDA), developed for random overlayers[9] is extended to the case of surfaces of random alloys with varying concentration profile near the surface. The non-self-consistent version of this approach was presented recently.[10] Both papers are in close relation to the formalism of effective multisite interactions for semi-infinite systems.[6] In the following, detailed reference is made to Refs. 6 and 10, which in turn will be referred to as I and II.

II. FORMALISM

The approach uses the all-electron tight-binding linear-muffin-tin-orbital (TB-LMTO) method,[11] which takes advantage of the short-range character of intralayer and interlayer interactions[12] to evaluate the surface Green's

function needed for a proper description of the electronic structure of semi-infinite random alloys. In the following it is assumed that from a certain layer on the electronic properties of all subsequent layers are those of the corresponding infinite system, which is either a homogeneous bulk alloy or the vacuum. The vacuum region is described by so-called empty spheres characterized by flat potentials representing the continuation of the semi-infinite lattice into the vacuum region. The whole system is therefore considered to be divided into three regions, namely (i) a homogeneous bulk alloy, (ii) a (homogeneous) vacuum, and (iii) an intermediate region consisting of several (M) atomic layers, where all chemical and electronic inhomogeneities are concentrated, and a few empty layers on top of the surface. Only potentials in the intermediate region are determined self-consistently while those for the homogeneous bulk alloy or vacuum are equal to the self-consistent potentials for the corresponding infinite systems (apart from the shift of the vacuum flat potential due to the electrostatic dipole barrier).

According to Eqs. (1) and (2) of I, the configurationally averaged Green's function is given by

$$\bar{g}(z) = \langle [P(z) - S]^{-1} \rangle = [\mathcal{P}(z) - S]^{-1}, \tag{1}$$

where S is the screened structure constant matrix and $\mathcal{P}(z)$ is the layer-dependent, site-diagonal coherent-potential function matrix, which due to the semi-infinite geometry refers in each particular layer p randomly to the corresponding potential function matrices of components A and B, $P_p^A(z)$ and $P_p^B(z)$, respectively. By neglecting relaxations of the top layers, the ideal bulk interlayer distances can be assumed throughout all three above-mentioned regions, and the screened bulk structure constants can be used. In these three regions, $\mathcal{P}(z)$ is of the following form:

$$\mathcal{P}(z) = \begin{cases} \mathcal{P}_p^v(z) = \mathcal{P}^v(z) & \text{for vacuum region} \\ \mathcal{P}_p(z),\ p = 1, 2, ..., M & \text{in the intermediate region} \\ \mathcal{P}_p^a(z) = \mathcal{P}^a(z) & \text{for bulk alloy layers,} \end{cases} \tag{2}$$

where $\mathcal{P}^v(z)$ and $\mathcal{P}^a(z)$ are determined from charge self-consistent bulk TB-LMTO-CPA calculations.[11] The coherent-potential functions $\mathcal{P}_p(z)$, $p = 1, 2, \ldots, M$, are found from a set of coupled CPA equations [see Eqs. (3) of I] for the layers in the intermediate region

$$\begin{aligned} &\sum_{\alpha=A,B} c_p^\alpha t_p^\alpha(z) = 0, \\ &t_p^\alpha(z) = [P_p^\alpha(z) - \mathcal{P}_p(z)]\{1 + \Phi_p(z)[P_p^\alpha(z) - \mathcal{P}_p(z)]\}^{-1}, \end{aligned} \tag{3}$$

where c_p^α are the layer-dependent concentrations of atom α which are generally different from the bulk concentrations c_b^α. For a particular site $\mathbf{R}_p$ in the layer p, the quantities $t_p^\alpha(z)$, $\alpha = A, B$, are the single-site t matrices of components A and B, and the quantity $\Phi_p(z) = \bar{g}_{\mathbf{R}_p\mathbf{R}_p}(z)$, the key quantity of the present theory, is the site-diagonal configurationally averaged Green's function [see Eqs. (18)–(21) of II]. The layer- and component-resolved charge densities $\rho_p^\alpha(\mathbf{r})$, $\alpha = A, B$, are then defined by

$$\rho_p^\alpha(\mathbf{r}) = \rho_p^{\alpha,\mathrm{core}}(r) + \sum_{L,L'} \int^{E_F} \chi_{pL}^\alpha(\mathbf{r}, E) \left\{ -\frac{1}{\pi} \operatorname{Im} F_{p,LL'}^\alpha(E + i0) \right\} \chi_{pL'}^\alpha(\mathbf{r}, E)\, dE, \tag{4}$$

where the $\chi_{pL}^\alpha(\mathbf{r}, E) = R_{pl}^\alpha(r, E)\, Y_L(\hat{\mathbf{r}})$ are partial waves, E_F is the bulk alloy Fermi energy, and $\rho_p^{\alpha,\mathrm{core}}(r)$ is the spherically symmetric core charge density. According to Eq. (30) of II, the matrix elements of the conditionally averaged Green's function $F_p^\alpha(z)$ are given by

$$F_{p,LL'}^\alpha(z) = \left[\frac{dP_{pL}^\alpha(z)}{dz}\right]^{1/2} (\{P_p^\alpha(z) - \mathcal{P}_p(z) - [\Phi_p(z)]^{-1}\}^{-1})_{LL'} \left[\frac{dP_{pL'}^\alpha(z)}{dz}\right]^{1/2}. \tag{5}$$

The radial amplitudes $R_{pl}^\alpha(r, E)$ are regular solutions of the radial Schrödinger equation. They are normalized to unity within a given atomic sphere (atomic-sphere approximation), and correspond to the spherically symmetric potentials

$$V_p^\alpha(r) = -\frac{2Z^\alpha}{r} + V_p^{\alpha,H}[\bar{\rho}_p^\alpha(r)] + V_p^{\alpha,\mathrm{xc}}[\bar{\rho}_p^\alpha(r)] + V_p^{\mathrm{Mad}}, \tag{6}$$

where

$$\begin{aligned} V_p^{\mathrm{Mad}} &= \sum_L \sum_q M_{pq}^{sL} \bar{Q}_q^L, \\ \bar{Q}_p^L &= \sum_{\alpha=A,B} c_p^\alpha \left(\frac{\sqrt{4\pi}}{2l+1} \int_0^{s^\alpha} r^l Y_L(\hat{\mathbf{r}})\, \rho_p^\alpha(\mathbf{r})\, d\mathbf{r} - Z^\alpha \delta_{l,0} \right), \end{aligned} \tag{7}$$

and Z^α is the atomic number of a component $\alpha =$

A, B. The first three terms in Eq. (6) represent the Coulomb potential of a point nucleus, the Hartree and the exchange-correlation terms, respectively, corresponding to the spherically symmetric part $\tilde{\rho}_p^\alpha(r)$ of the charge density $\rho_p^\alpha(\mathbf{r})$. The last term in Eq. (6) is the Madelung contribution for the pth layer as defined in terms of generalized intralayer and interlayer Madelung constants M_{pq}^{sL} (see Appendix). The quantity $\bar{Q}_p^L$ is the configurationally averaged multipole moment of the nonspherical charge density $\rho_p^\alpha(\mathbf{r})$ in the pth layer. Presently not only the monopole term from the net charges ($\bar{q}_p = \bar{Q}_p^{l=0}$) but also the contributions from the dipole moments ($\bar{d}_p = \sqrt{3}\,\bar{Q}_p^{l=1,m=0}$) corresponding to a polar vector $\hat{\mathbf{r}}$ perpendicular to the surface, are included.[13] The Madelung potential can be viewed as a spherically averaged potential field in a particular sphere generated by monopoles and dipoles at all other sites. Similarly, the electrostatic dipole barrier has contributions both from the net charges and from the dipole moments.

III. NUMERICAL RESULTS AND DISCUSSION

The above formalism is applied here to the case of the (001) surface of $Cu_{1-x}Ni_x$ fcc random alloys for uniform and nonuniform concentration profiles near the surface. In the present calculations the intermediate region consists of three atomic layers of the random alloy plus two layers of empty spheres. In this region the potentials are varied until in two consecutive iterations the maximum difference of all potentials under consideration was less than 0.005 Ry. The charge density of core electrons $\rho_p^{\alpha,\mathrm{core}}(r)$ is recalculated in each LDA step instead of applying the usual frozen-core approximation.[13] This, of course, is of little importance for the resulting valence charge densities, but can be of quite some importance for core-level shifts or for hyperfine magnetic fields. The local exchange functional is that of Ceperley and Alder[14] as parametrized by Perdew and Zunger.[15] For the $\mathbf{k}$-space integration 21 special $\mathbf{k}_\parallel$ points[16] are used in the irreducible ($\frac{1}{8}$th) part of the surface Brillouin zone (SBZ) of the fcc(001) face.

The charge self-consistent bulk TB-LMTO-CPA calculations were actually performed by coupling the ideal "left" and "right" semi-infinite alloys.[9] The result is, of course, the infinite bulk alloy. In this way, a maximum internal consistency for the bulk and the surface calculations can be obtained. It turned out that charge neutrality in the intermediate region was preserved within an accuracy of 10^{-3} electrons. Typically 0.25 electrons were found in the first empty sphere neighboring the surface. This charge gives rise to a lowering of the potential at the vacuum side (imagelike potential).

The results for the layer- and component-resolved densities of states (DOS) for the homogeneous concentration profile are presented in Figs. 1–5. In all cases the corresponding bulk DOS's are given for comparison. The layer DOS's of pure Cu (Fig. 1) and Ni (Fig. 5) show a characteristic narrowing in the surface layer due to the reduction of the number of nearest neighbors from 12 in the bulk to 8 at the surface. The DOS's at the third layer are already close to the corresponding bulk DOS's. As a result of charge self-consistency, the center of gravity of the surface DOS is shifted towards higher energies thus giving rise to a characteristic triangular shape of the DOS. Similar results were obtained for the related case of the Ag(001) surface.[9,17] The Cu and Ni DOS dif-

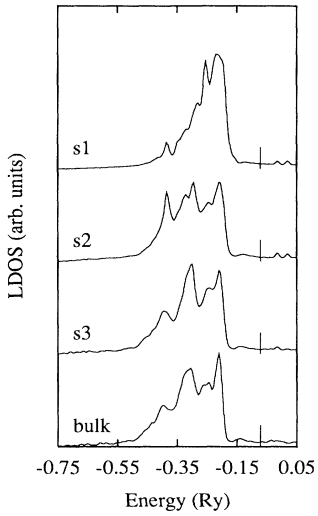

FIG. 1. Layer-resolved densities of states for a clean Cu(001) surface. The top three layers are denoted by $s1$, $s2$, and $s3$, respectively. The bulk density of states is given for comparison. The vertical lines denote the position of the bulk Fermi level.

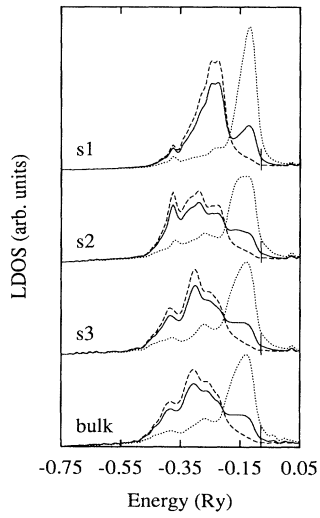

FIG. 2. Layer-resolved densities of states for a $Cu_{75}Ni_{25}(001)$ surface with a homogeneous concentration profile. The top three layers are denoted by $s1$, $s2$, and $s3$, respectively. The bulk alloy densities of states are given for comparison. The total densities of states (full lines), and the componentlike densities of states for Cu (dashed lines) and Ni (dotted lines) are shown. The vertical lines denote the position of the bulk alloy Fermi level.

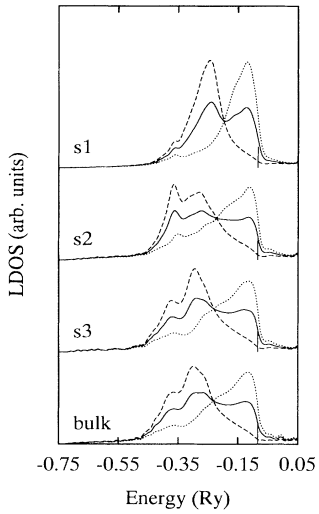

FIG. 3. Layer-resolved densities of states for a $Cu_{50}Ni_{50}(001)$ surface with a homogeneous concentration profile. The top three layers are denoted by $s1$, $s2$, and $s3$, respectively. The bulk alloy densities of states are given for comparison. The total densities of states (full lines), and the componentlike densities of states for Cu (dashed lines) and Ni (dotted lines) are shown. The vertical lines denote the position of the bulk alloy Fermi level.

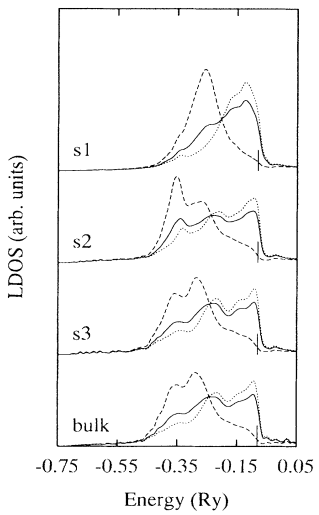

FIG. 4. Layer-resolved densities of states for a $Cu_{25}Ni_{75}(001)$ surface with a homogeneous concentration profile. The top three layers are denoted by $s1$, $s2$, and $s3$, respectively. The bulk alloy densities of states are given for comparison. The total densities of states (full lines), and the componentlike densities of states for Cu (dashed lines) and Ni (dotted lines) are shown. The vertical lines denote the position of the bulk alloy Fermi level.

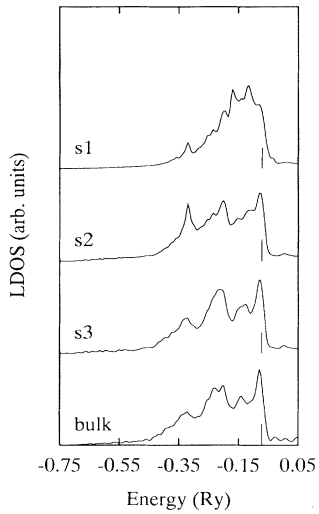

FIG. 5. Layer-resolved densities of states for a clean Ni(001) surface. The top three layers are denoted by $s1$, $s2$, and $s3$, respectively. The bulk density of states is given for comparison. The vertical lines denote the position of the bulk Fermi level.

fer by their bandwidths, the position of the Fermi level, and, in particular, by the relative position of the d-band centers on the energy axis. The latter effect has important consequences for the disorder in this alloy system. It should be noted that even if the peak at E_F in the surface Ni-DOS is suppressed in comparison with the bulk case, the value of the DOS at E_F is essentially unchanged due to surface band narrowing. The results for $Cu_{75}Ni_{25}$, $Cu_{50}Ni_{50}$, and $Cu_{25}Ni_{75}$ are presented in Figs. 2–4. The Cu-rich case shows a well-pronounced Ni virtual bound state close to the Fermi level as observed in the photoemission spectra,[18] and as obtained in previous non-self-consistent bulk calculations.[19–21] This peak is a consequence of the above-mentioned splitting between the Cu and Ni d levels. The presence of the surface shows up in an overall narrowing of the local Cu and Ni DOS and as compared with the bulk case leads to a more pronounced separation of the Ni-impurity peak from the main alloy band. The third layer is already bulklike which justifies, *a posteriori*, the number of layers chosen in the intermediate region. It is interesting to compare the local Cu-DOS in $Cu_{75}Ni_{25}$ with that for pure Cu. One can see a close similarity between both curves for energies below -0.25 Ry. For energies above -0.25 Ry, however, the shape of the layer Cu-DOS's is strongly modified by disorder when compared with the case of pure Cu. The Ni-rich alloy (Fig. 4) shows a common d band with no splitoff Cu peak. The reason for this behavior which is different from the Cu-rich case is the strong hybridization of the impurity Cu states with the host Ni states, since the Cu d band coincides energetically with the Ni d band. The Ni component layer DOS's resemble the corresponding DOS's of pure Ni(001) over the entire energy range, and

the effect of disorder appears only as smearing of the pure crystal features.

In the following the results for $Cu_{50}Ni_{50}(001)$ with the homogeneous concentration profile (Fig. 3) are compared to those for the inhomogeneous profile (Fig. 6). The inhomogeneous concentration profile used in the present calculations (Fig. 6) is based on the Monte Carlo simulations for a surface Ising model[6] at T=800 K.[8] It should be noted that such strong Cu segregation at the surface was observed experimentally[4] and was studied theoretically using various approaches.[1–4,22,23] As one can see in Fig. 6 the segregation of Cu atoms in the surface layer strongly influences the electronic structure. The top layer is essentially a monolayer of Cu atoms. The corresponding total DOS is quite similar to that of pure Cu(001) and is very different from that for the homogeneous profile. In the segregated case the alloy composition in the second layer still deviates from the bulk composition, and non-negligible differences from the homogeneous case are visible, especially for the local Cu and Ni DOS. In the third layer the differences between the homogeneous and the inhomogeneous case are negligible. The results indicate the importance of the surface composition for a proper interpretation of experiments mapping the DOS in near-surface regions such as, for example, photoemission or Auger-electron spectroscopy.

The most detailed information on the electronic structure of disordered surfaces can be obtained from layer-resolved Bloch spectral functions $A_p(\mathbf{k}_\parallel, E)$, which are given by the imaginary part of the $\mathbf{k}_\parallel$- and layer-resolved configurationally averaged Green's function [see Eq. (26) of II]. For $Cu_{75}Ni_{25}(001)$ these functions are presented in Fig. 7 for the case of $\mathbf{k}_\parallel = 0$ ($\bar{\Gamma}$ point in the SBZ) together with the corresponding quantities for the pure Cu(001) surface. For $E \leq -0.25$ Ry the shape of the Bloch spectral densities is only weakly influenced by disorder (smearing of peaks and small shift in energies). In the energy region close to the Fermi level, however, one can see the appearance of an extra structure, which is strongly smeared out by disorder, and which is due to impurity Ni atoms. In this energy regime the electronic states are strongly influenced by disorder. Simplified treatments using the virtual-crystal approximation would therefore definitely fail to describe the electronic structure for this system properly.

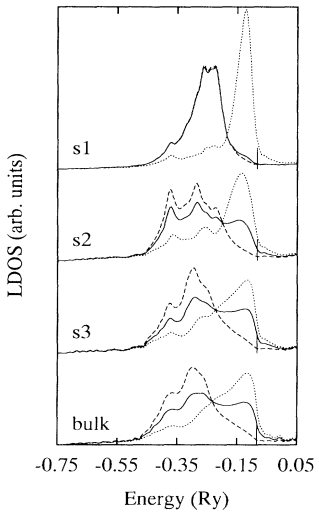

FIG. 6. Layer-resolved densities of states for a $Cu_{50}Ni_{50}(001)$ surface with an inhomogeneous concentration profile. The compositions in the top three layers $s1$, $s2$, and $s3$ are $Cu_{97}Ni_3$, $Cu_{63}Ni_{37}$, and $Cu_{48}Ni_{52}$, respectively. The bulk alloy densities of states are given for comparison. The total densities of states (full lines), and the component-like densities of states for Cu (dashed lines) and Ni (dotted lines) are shown. The vertical lines denote the position of the bulk alloy Fermi level.

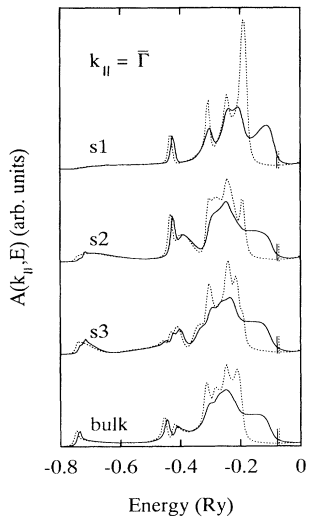

FIG. 7. $\mathbf{k}_\parallel = 0$ layer-resolved Bloch spectral densities for a $Cu_{75}Ni_{25}(001)$ surface with a homogeneous concentration profile. The top three layers are denoted by $s1$, $s2$, and $s3$, respectively. The corresponding spectral densities for a clean Cu(001) surface are shown as dotted lines. The vertical lines denote the position of the bulk alloy Fermi level (full lines) and the Fermi level of bulk Cu (dotted lines).

In Table I the work functions Φ as calculated from the expression $\Phi = B_{\text{dip}} - E_F$ are presented, where B_{dip} denotes the electrostatic dipole barrier calculated as described in the Appendix. The results for the clean Cu(001) and Ni(001) surfaces agree well with recent extensive theoretical calculations of work functions for all transition metals[24] using an approach[13] closely related to the present one. As discussed there, the calculated work functions are slightly higher (about $\leq 10\%$) in comparison with the experimental data as well as with those

TABLE I. Calculated work functions (eV) for the (001) surface of random CuNi alloys compared with available experimental data (Ref. 25).

	Cu	$Cu_{75}Ni_{25}$	$Cu_{50}Ni_{50}$	$Cu_{25}Ni_{75}$	Ni
This work	5.22	5.41	5.53	5.65	5.72
Experiment	4.59				5.22

obtained from full-potential slab[17] or supercell[26] calculations. On the other hand a recent full-potential surface Green's-function calculation[27] for Ni(001) gave a work function in accordance with the present calculations. Full-potential slab or supercell methods describe the charge density rather accurately and thus give a more reliable value of the dipole barrier $B_{\rm dip}$ as compared with the present approach. The Fermi level, which is a property of the infinite solid, is determined within the supercell or slab methods less accurately than in a Green's-function method for a semi-infinite system. Quite clearly, the work function depends on both the Fermi level and the dipole barrier.

The alloy work functions corresponding to the homogeneous concentration profile (Table I) increase monotonically with the Ni content. This is in agreement with the higher value of the Ni work function. The concentration dependence of the work function is slightly nonlinear. For $Cu_{50}Ni_{50}$ we have calculated also the work function for the inhomogeneous concentration profile corresponding to the results shown in Fig. 6. In this case the calculated value for the work function, namely 5.24 eV, is essentially the same as that for a clean Cu surface. This illustrates the strong dependence of the work function of an alloy with respect to the surface composition.

IV. SUMMARY

We have developed an efficient surface Green's-function method to calculate self-consistently electronic properties of disordered alloys with an inhomogeneous concentration profile at the surface within the tight-binding linear-muffin-tin-orbital method, whereby chemical disorder is described in terms of the coherent-potential approximation. The theory was applied to evaluate layer- and component-resolved densities of states, layer-resolved Bloch spectral densities, and work functions for disordered $Cu_{1-x}Ni_x(001)$ alloys for the homogeneous alloy compositions as well as for the case of a strongly inhomogeneous profile corresponding to a segregation of Cu atoms at the surface. The results indicate a pronounced dependence of the electronic properties of alloy surfaces on the composition of the top surface layers. Electronic structure calculations of this kind can be used as a starting point for statistical mechanic studies in terms of an Ising model and therefore for a study of surface phase diagrams or of surface segregation phenomena. An example of this type, a study of the surface segregation in CuNi alloys, is presented in Ref. 8.

ACKNOWLEDGMENTS

Financial support for this work was provided by the Academy of Sciences of the Czech Republic (Project No. 11015), the Natural Sciences and Engineering Research Council of Canada, the Austrian Ministry of Science (Project No. GZ 45.123./1-II/A/4/91), and the Austrian Science Foundation (P8918). One of us (J.K.) acknowledges the kind hospitality during his stay at Brock University, where the essential part of this work was carried out.

APPENDIX: MADELUNG CONSTANTS

For monopoles and dipoles perpendicular to a particular layer, the electrostatic potentials needed to evaluate the Madelung constants can be calculated by means of a simple two-dimensional (2D) Ewald technique. In the following, the simplest case, namely one atom per the 2D primitive cell, is considered. The origin of the coordinate system refers to the position of an arbitrary lattice point in this layer. The position vector $\mathbf{r}$ of a general point is denoted by $(\mathbf{r}_\parallel, r_\perp)$, where $\mathbf{r}_\parallel$ is a vector parallel to the layer and $r_\perp$ is a perpendicular component.

A Fourier transform of the difference between the potential produced by unit point sources (monopoles and dipoles) and the potential from the uniform compensating surface sources yields for $r_\perp \neq 0$ the following expressions for the monopoles:

$$\varphi(\mathbf{r}_\parallel, r_\perp) = \frac{4\pi}{\Omega} \sum_{\mathbf{G}_\parallel \neq 0} \frac{\exp(-|r_\perp||\mathbf{G}_\parallel|)}{|\mathbf{G}_\parallel|} \cos(\mathbf{G}_\parallel \cdot \mathbf{r}_\parallel) \tag{A1}$$

and the dipoles

$$\begin{aligned}\psi(\mathbf{r}_\parallel, r_\perp) &= -\frac{\partial}{\partial r_\perp}\phi(\mathbf{r}_\parallel, r_\perp) \\ &= \frac{4\pi}{\Omega}\,\mathrm{sgn}(r_\perp) \sum_{\mathbf{G}_\parallel \neq 0} \exp(-|r_\perp||\mathbf{G}_\parallel|) \\ &\qquad \times \cos(\mathbf{G}_\parallel \cdot \mathbf{r}_\parallel)\,. \end{aligned} \tag{A2}$$

Here Ω is the area of the 2D surface primitive cell and the $\mathbf{G}_\parallel$ are the reciprocal vectors of the 2D lattice. The sums in Eqs. (A1) and (A2) are absolutely convergent for $|r_\perp| > 0$. Equation (A1) is similar to a recent solution of the Poisson equation within the layer Korringa-Kohn-Rostoker method.[28]

The Ewald technique has to be used for points in the layer ($r_\perp = 0$). The electrostatic potential φ evaluated at the origin ($\mathbf{r} = \mathbf{0}$) is then given by

$$\begin{aligned}\varphi_0 = &-\frac{2}{\sigma\sqrt{\pi}} + \sum_{\mathbf{R}_\parallel \neq 0} \frac{2}{|\mathbf{R}_\parallel|}\,\mathrm{erfc}\left(\frac{|\mathbf{R}_\parallel|}{2\sigma}\right) \\ &- \frac{8\sigma\sqrt{\pi}}{\Omega} + \frac{4\pi}{\Omega} \sum_{\mathbf{G}_\parallel \neq 0} \frac{1}{|\mathbf{G}_\parallel|}\,\mathrm{erfc}(\sigma|\mathbf{G}_\parallel|)\,, \end{aligned} \tag{A3}$$

where $\mathbf{R}_\parallel$ denote the 2D lattice vectors, and

$$\mathrm{erfc}(x) = \frac{2}{\sqrt{\pi}} \int_x^\infty \exp(-t^2)\,dt\,. \tag{A4}$$

It should be noted that the singular contribution from the point charge located at the origin has not been included in φ_0, Eq. (A3), because only the intersite terms contribute to the Madelung field. The so-called Ewald parameter σ can be interpreted as the width of spherically symmetric Gaussian charge densities centered at the lattice points of the layer under consideration. Due to symmetry, the electrostatic potential ψ produced by dipoles is equal to zero for $r_\perp = 0$.

The total electrostatic potential $\chi(\mathbf{r}_\parallel, r_\perp)$ produced by

the net charges $\bar{q}_p = \bar{Q}_p^{l=0}$ and dipoles $\bar{d}_p = \sqrt{3}\,\bar{Q}_p^{l=1,m=0}$ of all M layers in the intermediate region can be constructed from the potentials φ and ψ using the superposition principle. If the total charge of these M layers is zero, the total electrostatic potential $\chi(\mathbf{r}_\parallel, r_\perp)$ goes to finite limits $\chi(\pm\infty)$ for $r_\perp \to \pm\infty$. In this case, the value $\chi(-\infty)$ that corresponds to a point deep inside the bulk can be taken as a reference value for electrostatic potentials. The electrostatic dipole barrier $B_{\rm dip}$ across the surface is then given by $B_{\rm dip} = \chi(+\infty) - \chi(-\infty)$ and the Madelung constants can be defined according to Ref. 13.

In general, the condition of charge neutrality cannot be fulfilled for a finite number of layers. Therefore, instead of the infinitely distant reference points $r_\perp = \pm\infty$, one has to take a reference point $(\mathbf{r}_{b\parallel}, r_{b\perp})$ in the bulk with finite $r_{b\perp}$ in order to determine the zero level of the potential $\chi(\mathbf{r}_\parallel, r_\perp)$, and a reference point $(\mathbf{r}_{v\parallel}, r_{v\perp})$ in the vacuum region with finite $r_{v\perp}$ to determine the dipole barrier. In the present calculation, we have taken the bulk (vacuum) reference point at a lattice site of the first bulk (vacuum) layer neighboring the intermediate region.

Let us denote the position of one lattice point in the pth layer as $(\mathbf{r}_{p\parallel}, r_{p\perp})$, where $r_{b\perp} < r_{p\perp} < r_{v\perp}$, $p = 1, 2, ..., M$. The Madelung contribution to the one-electron potential in the pth layer is then given by

$$V_p^{\rm Mad} = \sum_q (A_{pq}\bar{q}_q + B_{pq}\bar{d}_q) \tag{A5}$$

with the monopole-monopole Madelung constants

$$\begin{aligned} A_{pq} = \frac{4\pi}{\Omega}&(r_{q\perp} - r_{b\perp} - |r_{p\perp} - r_{q\perp}|) \\ &+(1-\delta_{pq})\varphi(\mathbf{r}_{p\parallel} - \mathbf{r}_{q\parallel}, r_{p\perp} - r_{q\perp}) \\ &+\delta_{pq}\,\varphi_0 - \varphi(\mathbf{r}_{b\parallel} - \mathbf{r}_{q\parallel}, r_{b\perp} - r_{q\perp})\,, \end{aligned} \tag{A6}$$

and the monopole-dipole Madelung constants

$$\begin{aligned} B_{pq} = \frac{4\pi}{\Omega}&[1 + (1-\delta_{pq})\,\mathrm{sgn}(r_{p\perp} - r_{q\perp})] \\ &+\psi(\mathbf{r}_{p\parallel} - \mathbf{r}_{q\parallel}, r_{p\perp} - r_{q\perp}) \\ &-\psi(\mathbf{r}_{b\parallel} - \mathbf{r}_{q\parallel}, r_{b\perp} - r_{q\perp})\,. \end{aligned} \tag{A7}$$

The electrostatic dipole barrier $B_{\rm dip}$ can be expressed similarly as

$$B_{\rm dip} = \sum_p (C_p\bar{q}_p + D_p\bar{d}_p), \tag{A8}$$

where the constants for the monopole and dipole contributions are given by

$$\begin{aligned} C_p = \frac{4\pi}{\Omega}&(2r_{p\perp} - r_{b\perp} - r_{v\perp}) + \varphi(\mathbf{r}_{v\parallel} - \mathbf{r}_{p\parallel}, r_{v\perp} - r_{p\perp}) \\ &-\varphi(\mathbf{r}_{b\parallel} - \mathbf{r}_{p\parallel}, r_{b\perp} - r_{p\perp})\,, \end{aligned} \tag{A9}$$

$$\begin{aligned} D_p = \frac{8\pi}{\Omega}&+ \psi(\mathbf{r}_{v\parallel} - \mathbf{r}_{p\parallel}, r_{v\perp} - r_{p\perp}) \\ &-\psi(\mathbf{r}_{b\parallel} - \mathbf{r}_{p\parallel}, r_{b\perp} - r_{p\perp})\,. \end{aligned} \tag{A10}$$

This approach represents a simple way of overcoming the problem of the charge neutrality for systems with a finite number of the self-consistently treated layers.

[1] F.L. Williams and D. Nason, Surf. Sci. **45**, 377 (1974).
[2] D. Kumar, A. Mookerjee, and V. Kumar, J. Phys. F **6**, 725 (1976).
[3] S. Mukherjee, J.L. Moran-Lopez, V. Kumar, and K.H. Bennemann, Phys. Rev. B **25**, 730 (1982).
[4] J. Eymery and J.C. Joud, Surf. Sci. **231**, 419 (1990).
[5] G. Treglia, B. Legrand, and F. Ducastelle, Europhys. Lett. **7**, 575 (1988).
[6] V. Drchal, J. Kudrnovský, L. Udvardi, P. Weinberger, and A. Pasturel, Phys. Rev. B **45**, 14 328 (1992).
[7] J. Kudrnovský, S.K. Bose, and V. Drchal, Phys. Rev. Lett. **69**, 308 (1992).
[8] A. Pasturel, V. Drchal, J. Kudrnovský, and P. Weinberger, Phys. Rev. B (to be published).
[9] J. Kudrnovský, I. Turek, V. Drchal, P. Weinberger, N.E. Christensen, and S.K. Bose, Phys. Rev. B **46**, 4222 (1992).
[10] J. Kudrnovský, P. Weinberger, and V. Drchal, Phys. Rev. B **44**, 6410 (1991).
[11] J. Kudrnovský and V. Drchal, Phys. Rev. B **41**, 7515 (1990).
[12] B. Wenzien, J. Kudrnovský, V. Drchal, and M. Šob, J. Phys. Condens. Matter **1**, 9893 (1989).
[13] H.L. Skriver and N.M. Rosengaard, Phys. Rev. B **43**, 9538 (1991).
[14] D.M. Ceperley and B.J. Alder, Phys. Rev. Lett. **45**, 566 (1980).
[15] J. Perdew and A. Zunger, Phys. Rev. B **23**, 5048 (1981).
[16] S.L. Cunningham, Phys. Rev. B **10**, 4988 (1974).
[17] H. Erschbaumer, A.J. Freeman, C.L. Fu, and R. Podloucky, Surf. Sci. **243**, 317 (1991).
[18] D.H. Seib and W.E. Spicer, Phys. Rev. B **2**, 1676 (1970).
[19] G.M. Stocks, R.W. Williams, and J.S. Faulkner, Phys. Rev. B **4**, 4390 (1971).
[20] G.M. Stocks, W.M. Temmermann, and B.L. Gyorffy, Phys. Rev. Lett. **41**, 339 (1978).
[21] S.V. Beiden, N.E. Zein, and G.D. Samolyuk, J. Phys. Condens. Matter **3**, 8597 (1991).
[22] M. Brejnak and P. Modrak, J. Phys. Condens. Matter **2**, 869 (1990).
[23] H.Y. Wang, R. Najafabadi, D.J. Srolovitz, and R. LeSar, Phys. Rev. B **45**, 12 028 (1992).
[24] H. Skriver and N.M. Rosengaard, Phys. Rev. B **46**, 7157 (1992).
[25] N.V. Smith and C.T. Chen, Phys. Rev. B **40**, 7565 (1989).
[26] M. Methfessel, D. Hennig, and M. Scheffler, Phys. Rev. B **46**, 4816 (1992).
[27] J. Inglesfield and G.A. Benesh, Phys. Rev. B **37**, 6682 (1988).
[28] J.M. MacLaren, S. Crampin, D.D. Vvedensky, and J.B. Pendry, Phys. Rev. B **40**, 12 164 (1989).